



HAL
open science

Parametric Study of Accidental Impacts on an Offshore Wind Turbine Composite Blade

Hicham Boudounit, Mostapha Tarfaoui, Dennoun Saifaoui, Yumna Qureshi

► To cite this version:

Hicham Boudounit, Mostapha Tarfaoui, Dennoun Saifaoui, Yumna Qureshi. Parametric Study of Accidental Impacts on an Offshore Wind Turbine Composite Blade. *Journal of Bio- and Tribo-Corrosion*, 2021, 7 (1), 10.1007/s40735-021-00473-z . hal-03151972

HAL Id: hal-03151972

<https://ensta-bretagne.hal.science/hal-03151972>

Submitted on 19 Jan 2023

HAL is a multi-disciplinary open access archive for the deposit and dissemination of scientific research documents, whether they are published or not. The documents may come from teaching and research institutions in France or abroad, or from public or private research centers.

L'archive ouverte pluridisciplinaire **HAL**, est destinée au dépôt et à la diffusion de documents scientifiques de niveau recherche, publiés ou non, émanant des établissements d'enseignement et de recherche français ou étrangers, des laboratoires publics ou privés.



Distributed under a Creative Commons Attribution - NonCommercial 4.0 International License

Parametric Study of Accidental Impacts on an Offshore Wind Turbine Composite Blade

Hicham Boudounit^{1,2} · Mostapha Tarfaoui² · Dennoun Saifaoui¹ · Yumna Qureshi²

Abstract

Wind turbine blades are the key components that allow the extraction of energy from the wind; these blades are often subjected to accidental impacts which usually occurs on moving blades with maintenance tools, hail, or flying birds, resulting in a significant degradation of the structural integrity of the blade. In this paper, a numerical simulation is adopted using finite element method (FEM) with ABAQUS software to investigate the mechanical behavior of a GRP composite wind turbine blade under low-velocity impact in operating conditions. On the other hand, damage modeling was formulated based on Hashin criteria for intra-laminar damage to detect failure modes in large wind turbine blade, the sensitive zones, and the size of damaged areas. To investigate this situation, a comparative evaluation was carried out considering many impact scenarios and the main parameters such as the impactor geometry, velocity, and weight. The results are then examined and analyzed, which show that major damage appeared at the tip of the blade and on trailing edge. Furthermore, the impactor geometry affects the type of damage, the weight affects the size of the damaged area, while the impact velocity influences the mechanical response of the composite wind turbine blade.

Keywords Impact · FEM · Mechanical behavior · Impactor shape · Damage · Hashin's criterion

Abbreviations

HSNFCCRT	Hashin criterion for fiber in compression	Y_C	Transverse compressive strength
HSNFTCRT	Hashin criterion for fiber in tensión	S_{LT}	Longitudinal shear strength
HSNMCCRT	Hashin criterion for matrix in compression	S_{TT}	Transverse shear strength
HSNMTCRT	Hashin criterion for matrix in tensión	$G_{fp}, G_{fc}, G_{mt}, G_{mc}$	Damage evolution coefficients
E_1	Longitudinal Young modulus	ALLAE	Artificial strain energy ALLIE: Total strain energy
E_2	Transversal Young modulus	ALLSE	Recoverable strain energy
E_3	Young modulus along the thickness	ALLMD	Energy dissipated by damage
$\nu_{12}, \nu_{13}, \nu_{23}$	Poisson's ratio	ALLKE	Kinetic energy
G_{12}	Shear modulus in 1–2 plane	ETOTAL	Energy balance
G_{13}	Shear modulus in 1–3 plane		
G_{23}	Shear modulus in 2–3 plane		
X_T	Longitudinal tensile strength		
X_C	Longitudinal compressive strength		
Y_T	Transverse tensile strength		

✉ Hicham Boudounit
hichamboudounit@gmail.com

¹ FSAC – UH2C, Laboratory for Renewable Energy and Dynamic Systems, Casablanca, Morocco

² ENSTA Bretagne, IRDL, UMR CNRS 6027, 29200 Brest, France

1 Introduction

Nowadays, wind energy is the world's most growing renewable energy resource [1]. According to the Renewable Energy Policy Network report, published in 2018 [2, 3], 75% of global energy demand is covered by fossil energy (oil, natural gas, and coal), resulting in an increase in greenhouse gases (GHGs) emitted into the atmosphere and consequently, global warming, which manifests as floods, hailstorms, cyclones, and heat waves [2]. The 25% left is covered by renewable energy resources with 36.9% for Hydropower [3],

31.8% for Windpower [3], 11.6% [3] for Solar power, and 19.7% [3] left for other renewable sources generation power.

Wind turbine blades are the most important components for wind energy conversion, their structure is designed to retrieve the kinetic energy from the wind while rotating and converting it to electrical energy with the help of a generator. In service, the blades are subjected to different types of loads such as aerodynamic, centrifugal, and gravity [4–8]. Botasso et al. [9] described a new aero-elastic model, which allows the active control of the couple and the pitch. It was used to perform experiments beyond aerodynamics on a horizontal axis wind turbine, and its efficiency is proven ; however, the model is unable to match the Reynolds number, which leads to a reduction of the power coefficient.

Moreover, Brøndsted et al. on their review [10] presented the different loads, Gravity, Aerodynamic, and Centrifugal, acting on the wind turbine during service and their effects on the rotating blades, and focused their study on the mechanical behavior of composite materials, advantageous performance, and damage mechanisms.

One of the most important steps for certification of wind turbine blades is predicting its durability by evaluating the damage evolution over the composite structure as well as its mechanisms. In order to understand the damage evolution in wind turbine blades under static and cyclic loadings, Sørensen et al. [11] carried a study using a combination of material and structural modeling. The results show that two types of damages (compression failure and crack growth) along adhesive joints, in addition, the effect of porosity on the strength of adhesive joints, were investigated by developing an approach for predicting their fracture mechanisms. On the other hand, Shokrieh and Rafiee estimated the degradation of the composite material properties used on wind turbine blade under static loads and predicted a lifetime of 18 to 24 years [12].

Montesamo et al. [13] developed and tested on a 32.5 m composite wind turbine blades, a new progressive damage model, which turned to be very efficient in controlling and predicting the most sensitive zones to damage and failure on the composite blade. Moreover, in 2018, they developed algorithms to assess the influence of plies interactions on the sliding displacement and on crack surface, and these expressions were coupled with a multistage damage model that allows predicting failure on laminates [14].

Yang et al. [15] carried a comparative study to investigate and evaluate the deformation as well as to identify the sensitive zones to failure on a large full-scale composite blade under flapwise loading. The results indicate that the damage began with the delamination of the aerodynamic shell from the adhesive joints, followed by an increase in the stress amplitude, which leads to an unstable propagation of damage then the collapse of the structure. In the same context, Overgaard and Lund [16, 17] conducted a comparative study

on the effect of static flapwise on wind turbine blades and developed an efficient model to predict the stiffness degradation and the damage evolution in laminates, which can be coupled with delamination models that allow assessing the durability of composite structures.

Wind turbine blades are subjected to different loads which impose large fatigue stresses on the moving rotor especially in the transition region of the blade [18] and can also be subjected to an accidental impact as traveler birds, the hail, or with a falling maintenance tool, and a small scratch on the blade can be fatal for the whole wind turbine structure [19]. Various researchers have studied the optimization of the layup parameters for a wind turbine blade in order to increase its aerodynamics and structural performance [20–26]. Others had studied the impact on composite structures as on a turbine nozzle [27, 28] and found that the damage evolution depends on the impactor geometry and speed.

On the other hand, Geubelle [29] studied the effect of the low-velocity impact on the delamination in thin composites plates using a 2D cohesive/volumetric finite element scheme. Then, Troussset [30] tested the effect of low-velocity impact on a laminated composite plate with the organic matrix to anticipate damage locations. Furthermore, Hamitouche et al. [31] developed a computational approach to predict mechanical damage in laminated composite structures. Pugh et al. had tested the effect of the bending stress and salinity on the erosion mechanisms of composite wind turbine blades [32, 33]. Ahamed et al. [34] tested the effect of impact angle on the erosion of composite materials for tidal applications.

Unlike metallic materials, the damage caused on a composite structure during impact is a major issue. They may have undergone stress, which can change the internal cohesion of the structure, but no visible damage on the surface [35]. According to Davies [36, 37], during the impact, an important part of the incident energy is absorbed in the form of fragmentation of the material, which is an essential parameter to understand the phenomenon generated during an impact on a composite structure. It determines the amount of available energy that can be absorbed by the target in the form of elastic deformation and damage and shows that at low velocity the damage is dominated by flexion; however, at high speed, the damages are more localized, because the deformation waves do not have enough time to propagate throughout the structure.

Given the three-dimensional nature of laminated composites, many parameters influence the nature of the damage. However, the major parameters are the initial speed of the impactor and weight. The response of the target will then depend on the combination of these parameters, which will generate different damage [38, 39]. Olsson [38] used a criterion based on the weight and the shape of the impactor to determine the nature of the response during an impact and found that the shape of the impactor affects the rate of

penetration into the structure, the peak strength, the contact time, and damage threshold. Mitrevski et al. [39] monitored the mechanical behavior of a composite plate during impact using four different impactor forms and found that the flat impactor did not leave a residual mark, but created defects that are difficult to detect; however, the conical impactor left the deepest indentation. In this framework, many researchers, such as Yamada-Sun [40], Hart-Smith [41], and Hashin [42], proposed different models to capture varying degrees of these damage mechanisms. Hashin's criterion uses more than one stress component to evaluate the different failure modes.

This work has been focused on examining the change of the structural properties and damage generated on large wind turbine blade under different impact scenarios. The problem of the design of wind turbine blades has been also treated using ABAQUS software based on the finite element method taking into account aerodynamic, centrifugal, and inertial loads under the conditions of service of the blade. The effect of the impactor geometry, weight, and impact velocity on the dynamic response and damage kinetics inducted to the wind turbine blade in service where they are investigated to improve the long-term structural integrity of composite wind turbine blades.

2 Experimental Tests and Numerical Model Validation

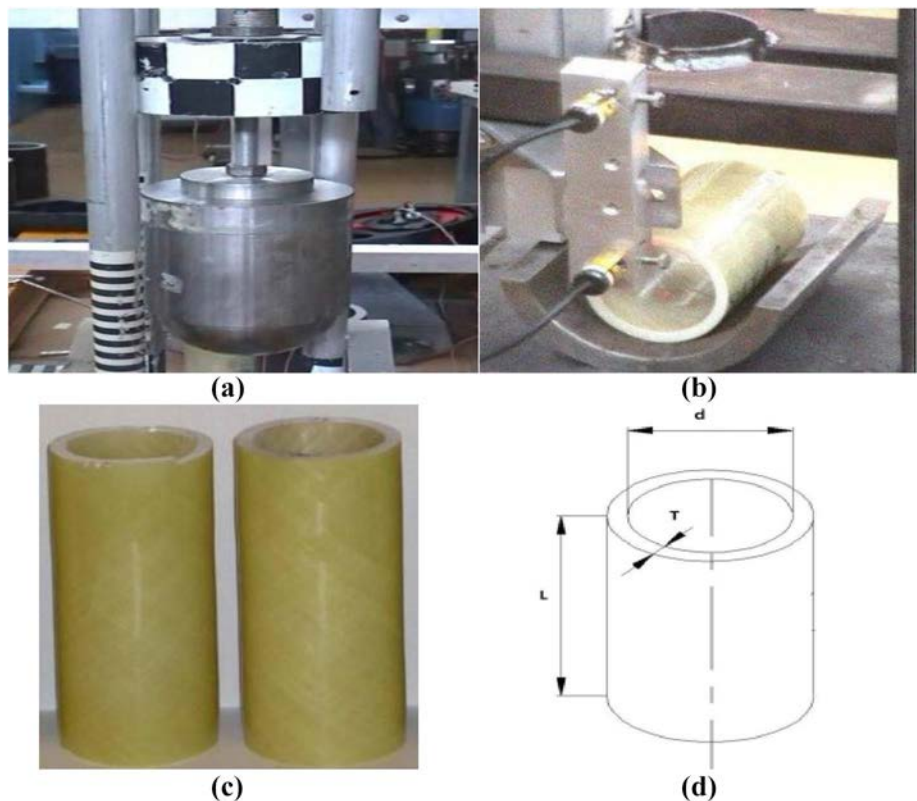
2.1 Experimental Tests

To study the mechanical behavior of the composite wind turbine blade shown in Figs. 1 and 2, under impact with birds, or hail, as well as to validate the developed VUMAT subroutine which gives the damage occurred on the wind turbine blade, numerical simulations and experimental tests are performed on a composite tubular specimen made by STRAGLEN co.

Impact tests were performed using IFREMER experimental bench on the composite tubular specimen, which has a surface much larger than that of the impactor. The tubular specimen with the dimensions are grouped in Table 1, and placed in a cradle as shown in Fig. 2. Furthermore, the specimen was made of glass fiber-reinforced polymer matrix composites with the mechanical properties of an E glass/epoxy fold presented in Table 2.

The assembly schematized in Fig. 1a consists of a tower from which a hemispherical projectile was dropped. The projectile has 50 mm diameter, 200 mm length, and 1.6 kg weight with a density ρ equal to 7800 kg/m^3 . The Young modulus (E) is equal to 210 MPa and Poisson coefficient (ν) is equal to 0.3. Furthermore, a piezoelectric accelerometer

Fig. 1 Experimental Bench



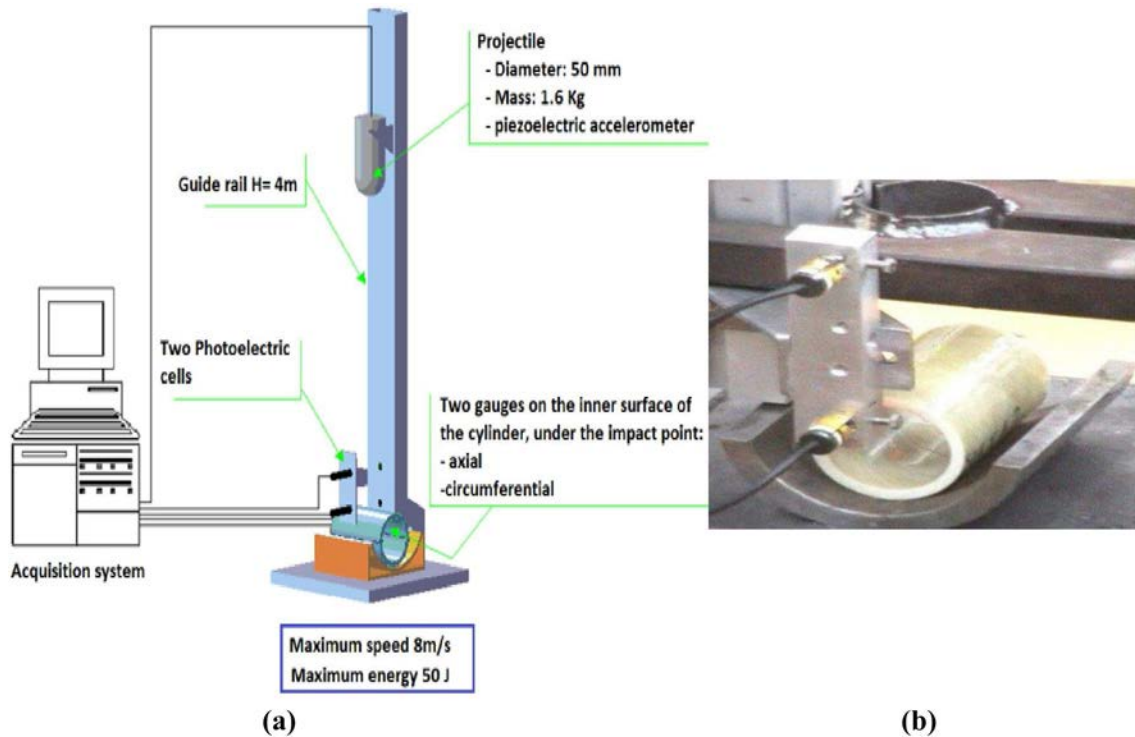


Fig. 2 The geometry of the cylinder and impactor

Table 1 Tube characteristic

Internal diameter D (mm)	Thickness T (mm)	Length L (mm)	Winding
55	6	200	$[\pm 55]_{10}$

ENDEVCO 2255B-1 is housed inside the hemispherical tip (about 10 mm from the point of contact with the tubular specimen). The experimental bench is also equipped with an anti-rebound device consisting of a self-triggering electromagnetic clamp, which prevents a second shock Fig. 1b.

The tube is placed in a cradle of 104 mm diameter, which is held rigidly to the frame, and the impact occurs at mid-length of the tubular specimen with normal incidence. Two photodiode sensors are placed few centimeters in front of the impact point, which allows the measurement of the incident velocity of the projectile.

When the projectile passes between the diodes and the light source, a breaking of the light beam is detected, which allows recording the impact velocity as well as defining the energy restored by the tube to the projectile; hence its rebound.

Some tubular specimen are equipped with two strain gauges disposed on the inner surface of the cylinder, axially and circumferentially under the impact point, which allows to measure strain rate during the tests. A fast camera

(FASTCAM APX) with a maximum acquisition rate of 120,000 frames per second was used to record the interaction between the projectile and the tubular specimen during the impact, as well as measuring of the projectile velocity and materials displacement.

NICOLET data acquisition unit was used to record the measurement, which is subsequently processed and analyzed using MAPLE and MATLAB software.

Figure 2a shows the impactor geometry, (b) represents the experimental bench, (c) real picture of the tube, and (d) represents the main parameters of the tubular specimen and are summarized in Table 1.

2.2 Numerical Simulation of Impact on Wind Turbine Blades

This study aims to evaluate the change of the structural properties, the type of damages, and the size of the damaged zone of a wind turbine blade in service under accidental impacts. For that effect, an impact study with different impact scenarios on the most vulnerable spots on the blade has been conducted using different impactor geometries (conical hemispheric), different weights, and different initial velocities.

A 48 m wind turbine blade, with box-shaped spars, was modeled as a deformable structure, while the impactor was modeled as a rigid body. The general specifications of the studied blade model are presented in Table 3.

Table 2 Mechanical properties of the E glass/epoxy fold

E_1 (MPa)	$E_2 = E_3$ (MPa)	ν_{12}	$\nu_{13} = \nu_{23}$	$G_{12} = G_{13}$ (MPa)	G_{23} (MPa)
48,160	11,210	0.274	0.096	4420	9000
X_T (MPa)	X_C (MPa)	Y_T (MPa)		Y_C (MPa)	$S_{LT} = S_{TT}$ (MPa)
1021.3	978	29.5		171.8	35.3
G_{11} (N/mm)	G_{1c} (N/mm)	G_{1t} (N/mm)	G_{1c} (N/mm)	G_{cc} (N/mm)	
0.3	0.3	0.6	0.6	0.6	
ρ (kg/m ³)		1900			

Table 3 Blade properties

Length (m)	48
Weight (tons)	13.95
Airfoil type	NACA 4424
Max chord (m)	3932
The maximum thickness of the profile as a percentage of the cord (%)	24
Position of the maximum thickness in cord percentage (%)	30
Angle of attack for maximum lift (deg)	7
Maximum coefficient of lift	1.08
Coefficient of drag at angle of attack of 7°	0.01

Figure 3 shows the wind turbine blade with various chord lengths and different twist angles.

The properties of the composite material used in the numerical simulation are listed in Table 1.

Figure 4a shows the stratification model used for the blade. (b) The distribution of materials in the zone [c] of the blade and (c) the distribution of the materials and their thickness with spars length.

Table 4 regroups the different orientations of different materials used in this study.

- Fig. 5 illustrates the boundary condition assigned to the blade using “Encastre” type applied at the root to reduce the computational requirements. The blade is fixed at one end to act as a cantilever, while the other end is free. (a) shows the boundary condition for the numerical model and (b) for the reel fixation of the wind turbine blades.
- The aerodynamic loads were calculated using the BEM code shown in Fig. 6, for a wind speed of 20 m/s, and applied to the structure as shown in Fig. 7, using a DLoad subroutine implemented in ABAQUS.
- Gravity load is computed by ABAQUS FEA software using the layup parameter of the blade.
- Fig. 8 shows the centrifugal force which is calculated using Eq. (1). It depends on the weight and the rotational velocity of the blade.

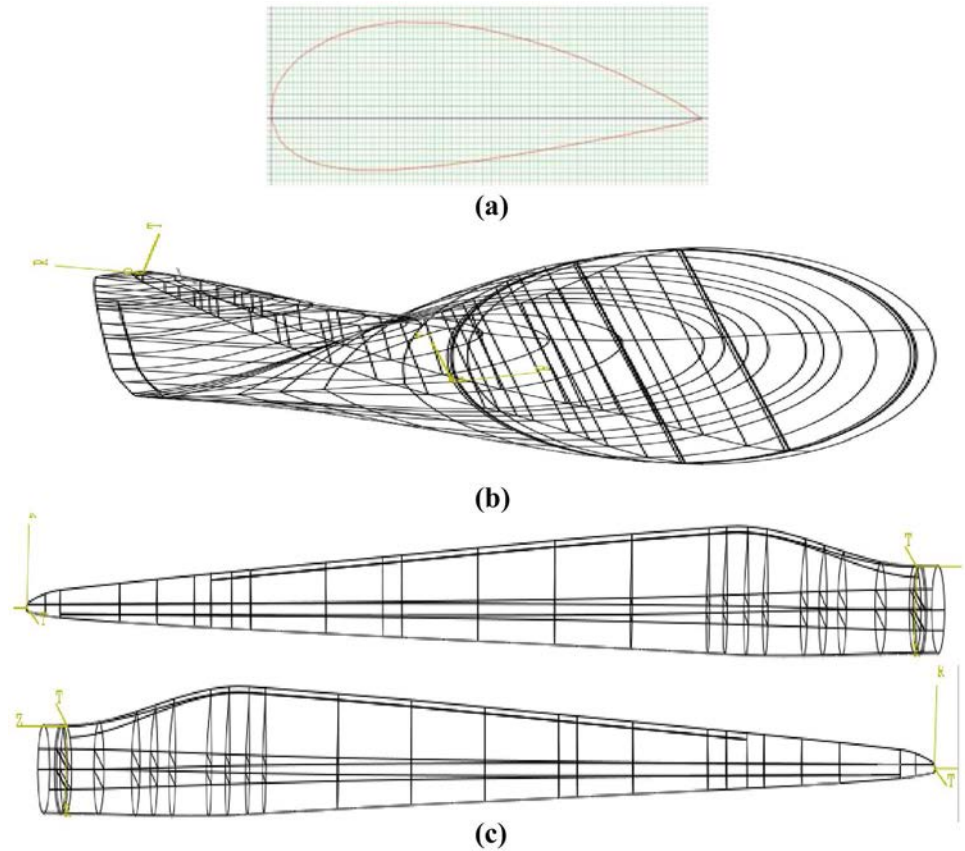
$$F_c = \frac{1}{2} m \omega^2 r \quad (1)$$

where ω is the rotational velocity and r is the distance of the blade element from the center of rotation. Equation (2) was used to calculate the centrifugal force on each element along the blade's length.

$$F_c = \frac{\omega^2}{2} \int m_s r dr \quad (2)$$

Figure 9a shows the blade under all loads where the green arrows are for centrifugal load and the purple ones are for

Fig. 3 The structural design of the blade



the aerodynamic load. Figure 9b is an enlargement of a section of the blade. The general specifications used during the study are listed in Table 5.

For a good design of the wind turbine blade, and to understand its behavior under dynamic loading, we conducted impact tests. The blade was exposed to different impactor geometries such as hemispherical and conical, Table 6. Parametric analysis is conducted which deals with the effect of the velocity, energy, and mass of the impactor.

- The impactor was modeled as a rigid body.
- The impact was occurred in the critical zones of the blade. Fig. 10a shows a view of the zones where the impact occurs: (b) the tip of the blade and (d) the trailing edge. Fig. 10c and e represent the layup parameters of these zones, respectively.
- Two types of impactors were used to compare the effect of the geometry.
- The effect of impact velocity was tested using different initial velocities for the impactor.
- The effect of impactor weight was studied using weights of 5 kg and 10 kg.

3 Results and Discussion

Figure 11 shows the occurrence of the damage on the tube with different impact energies. It must be noted that, at 3 J, no damage was observed on both sides of the target but, after reaching 5 J, a small damaged area with a little hole appeared on the external surface because of the nature of the impactor. Moreover, the damaged area was a bit larger at the inner surface. The increase in damaged area size and the penetration rate of the impactor became more important while increasing the impact energy.

Three tests for each impact energy were performed and Fig. 12 shows the reproducibility of the results. Figure 12a shows the evolution of impact force with time for all three tests and Fig. 12b shows the evolution of material displacement or the penetration of the impactor on the target as a function of time. Figure 13a shows the evolution of impact force with time and its dependence on the kinetic energy of the impactor. Moreover, Fig. 13b shows the penetration rate of the impactor on the composite tube which showed dependency on the initial energy of the projectile.

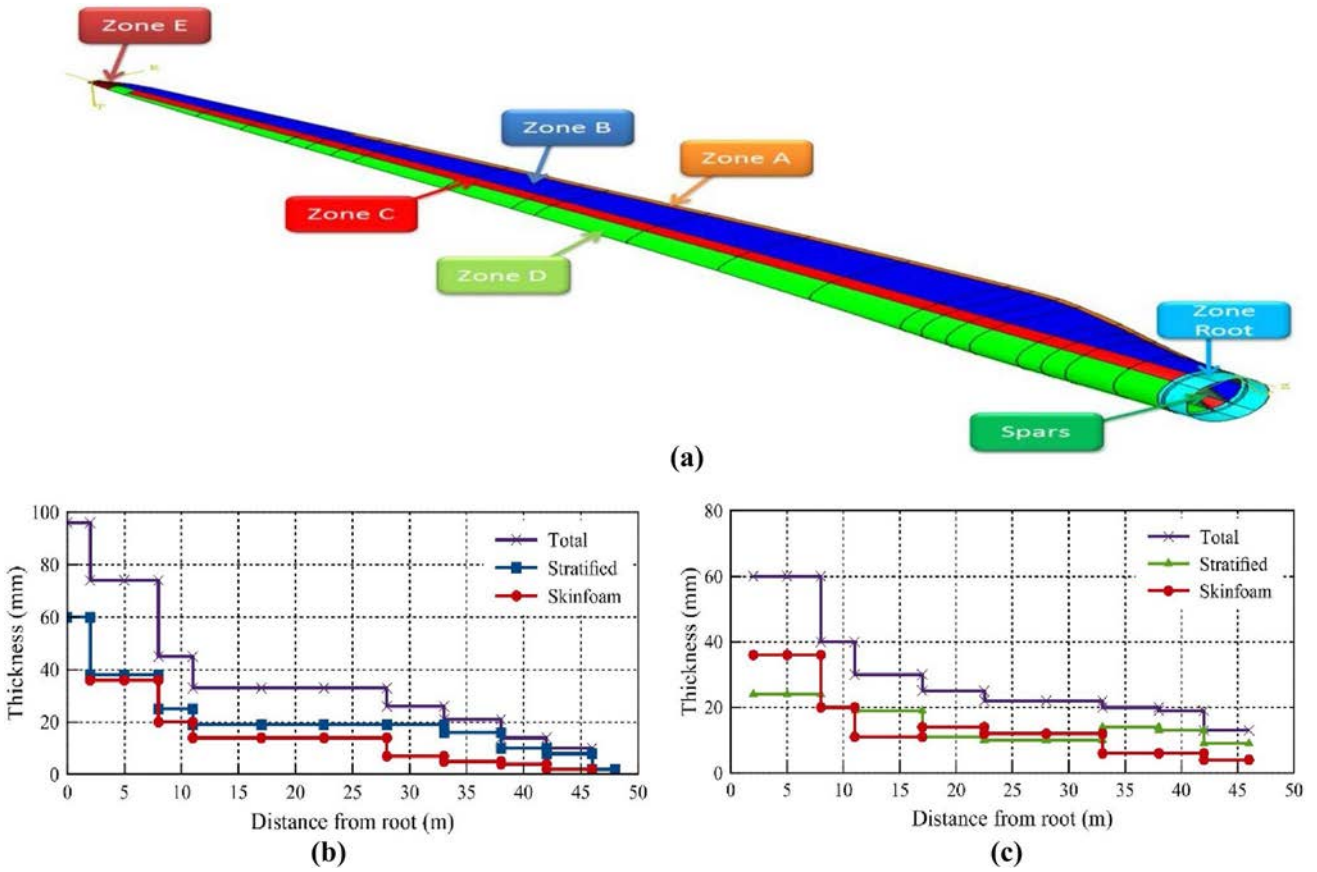


Fig. 4 Composite layup: distribution of materials and layup thickness

Table 4 Composite layup orientation

	Triax	UD	R4545
Orientations (°)	[-45/0/45]	0	[-45/45]

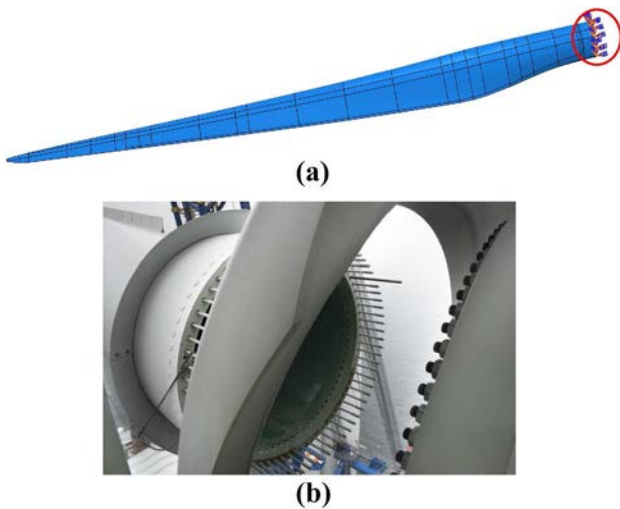


Fig. 5 Encastre Boundary condition

Numerical simulation of impact on the tubular structure with the same characteristics as shown in Fig. 14 and Table 7 was performed to verify the experimental results.

where C3D8R is Eight-node brick element with reduced integration.

The numerical simulation results show similarities with the experimental test in the mechanical behavior of the tubular specimen under impact, and Fig. 15 shows that the displacement and Force values found using the numerical simulation in ABAQUS correlate with the experimental tests. Furthermore, as for the experimental tests, the visualization of the numerical simulations displayed in Fig. 16 shows larger damaged area in the inner surface, but with less stress level than the external surface, as well as similarities in the size of the damaged zone for both sides. Thus, the VUMAT subroutine developed for impact study is validated.

A numerical simulation of a composite blade wind turbine under low-velocity impact using the VUMAT subroutine previously validated was preceded and the damage evolution on the wind turbine blade was monitored and quantified.

A mesh convergence study was carried out with different mesh sizes under the same loading and boundary conditions

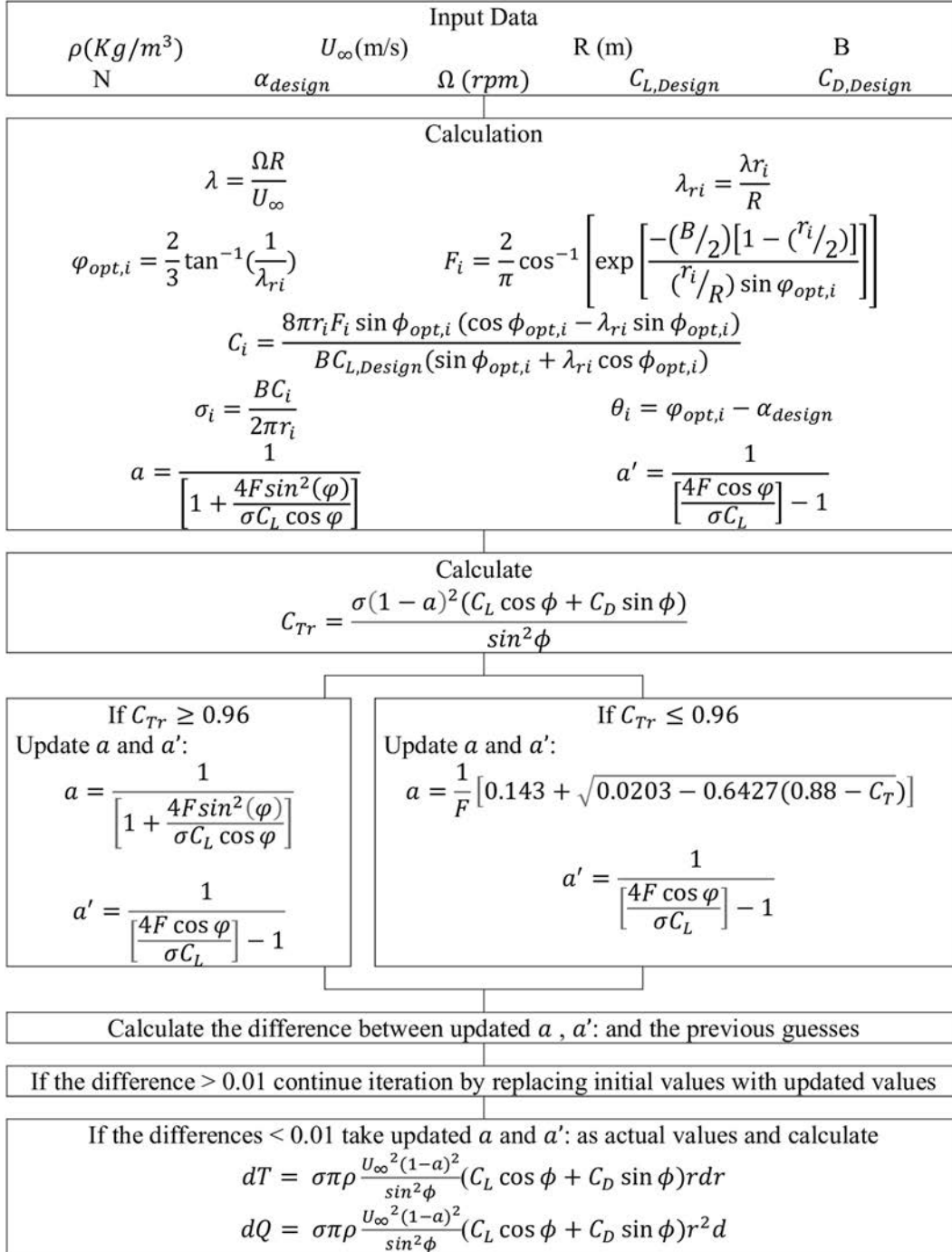


Fig. 6 BEM Algorithm for Dload Subroutine

to establish an interval of optimal mesh size, which gives accurate results with less calculation time, Fig. 17 and Table 8.

In this section, an analysis of the dynamic response and the damaged area of a wind turbine blade after impact loading with presence of aerodynamic loads is given. Examining

the results shown in Fig. 18, the theory of energy conservation of the system during impact tests was verified. Figure 18 shows the variation of energies during impact with a 5 kg hemispheric impactor at 20 m/s. The total energy (ETOTAL) was constant throughout the calculation time and corresponded to the addition of kinetic energy (ALLKE) and

Fig. 7 Distribution of aerodynamic load

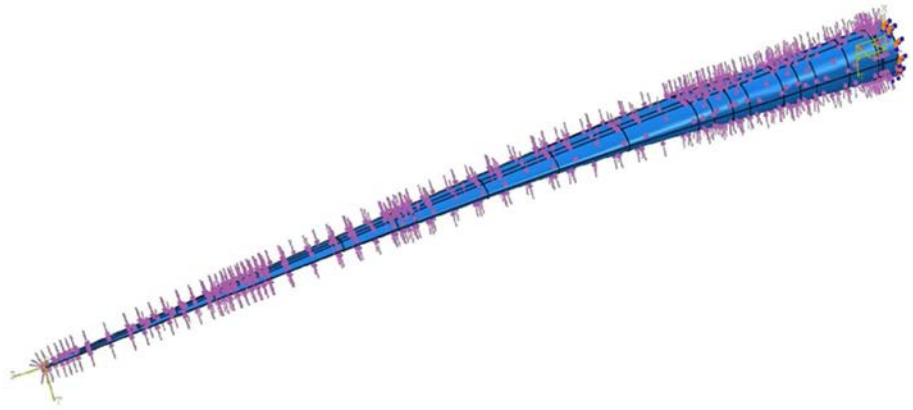


Fig. 8 Centrifugal load on the wind turbine blade

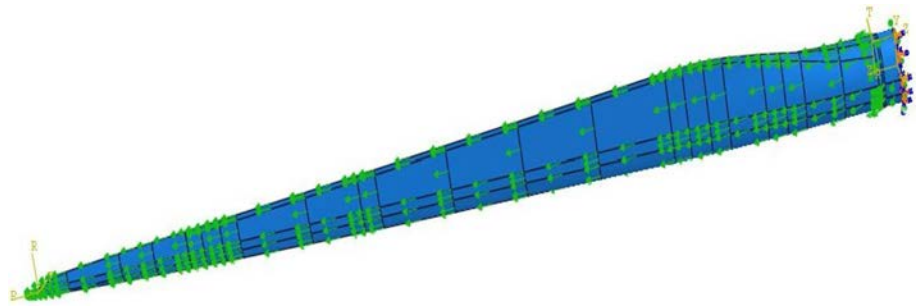


Fig. 9 Wind turbine blades in service

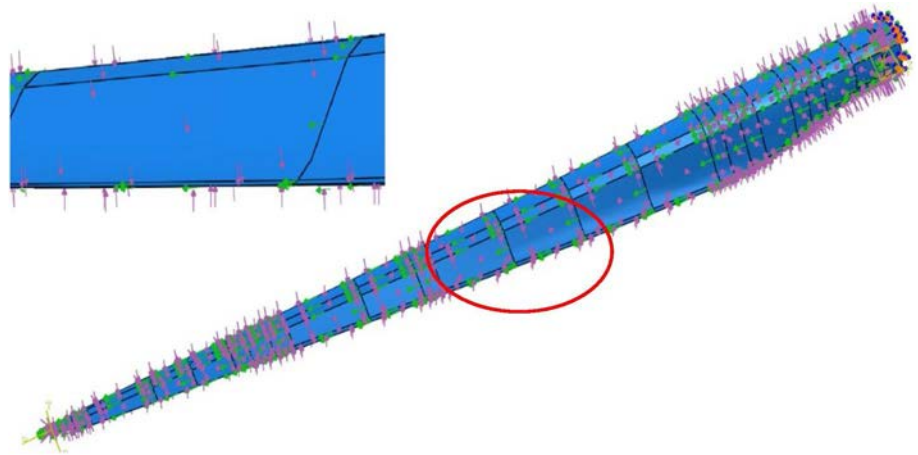


Table 5 Numerical simulation load parameters

Loads and boundary condition	Location	Magnitude
Encastre	Root of the blade	–
Aerodynamic	The whole structure	20 m/s
Centrifugal (angular velocity)	The whole structure	3.14 rad/s
Gravity	The whole structure	9.81 m/s ²

Table 6 Projectile property

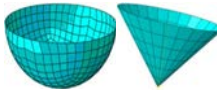
Impactor shape	Weight (kg)	Impact speed (m/s)	Kinetic energy [kJ]	Impact location
	5	15	0.562	16.0 m
	10	20	1.00	47.0 m
			1125	
			2.00	

Fig. 10 Impact locations on the blade

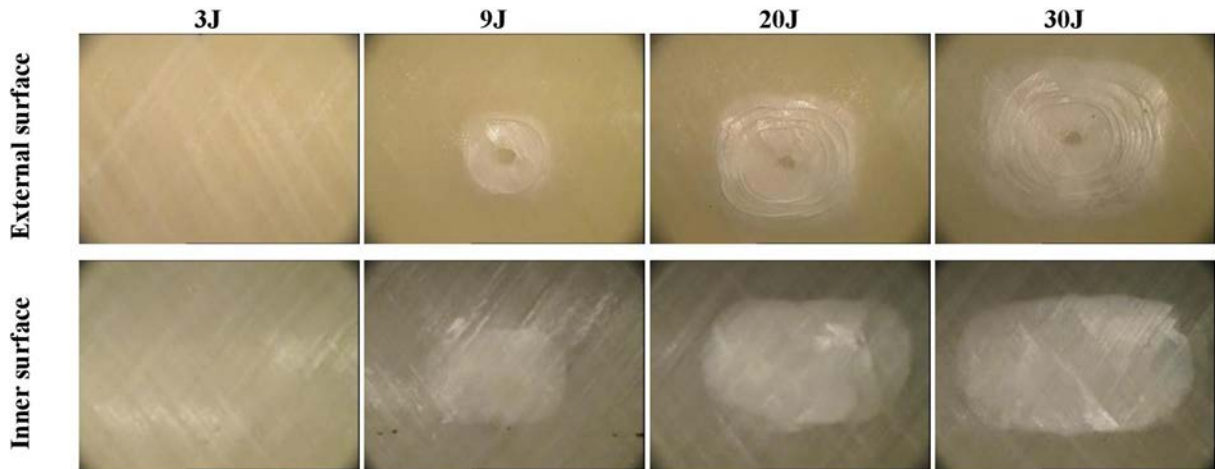
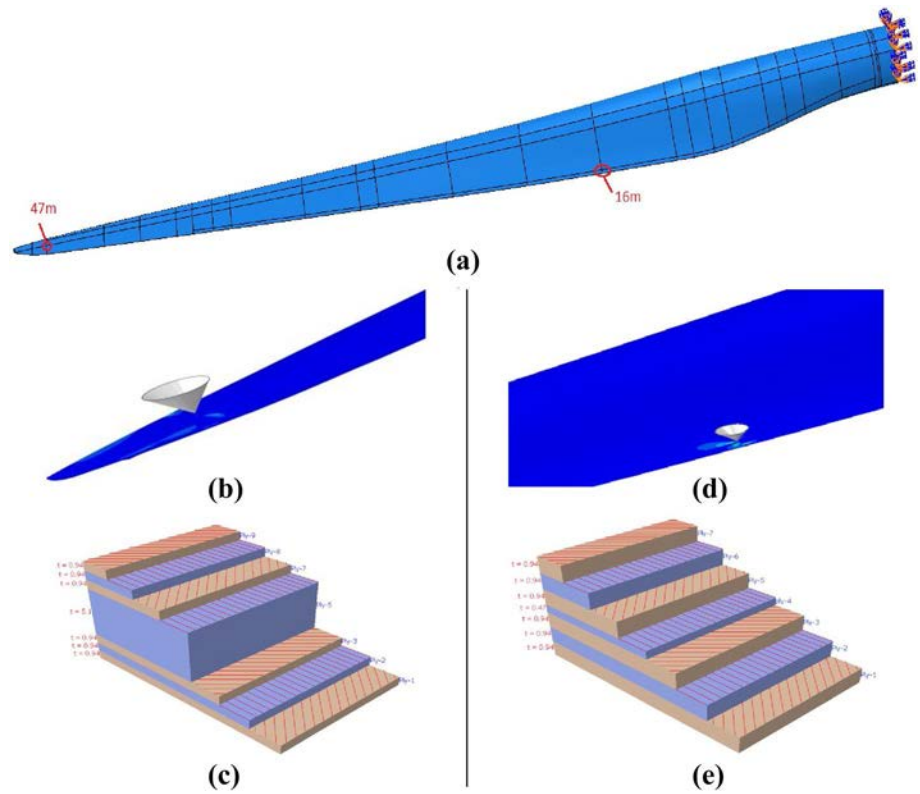


Fig. 11 Damage appearance on the inner and external surface

internal energy (ALLIE). The evolution of the deformation energy (ALLSE) had the same path as the internal energy. Furthermore, the internal energy correspond to the sum of the strain energy (ALLAE) and the energy dissipated by damage (ALLMD). Hence the conservation of energy during the impact test was verified.

In the previous section, the numerical model developed showed its efficiency when compared with the experimental results of the tubular specimen under impact. While this part

is focused on the damage appeared on a wind turbine blade during accidental impact with different impact scenarios, it should be noted that the damage is controlled by Hashin's criteria to estimate the fiber and matrix damage initiation and propagation.

The impact was performed on the trailing edge as well as at the tip of the blade because after the preliminary study it was found that these zones are the most sensitive to damage due to the absence of spars and to their thickness.

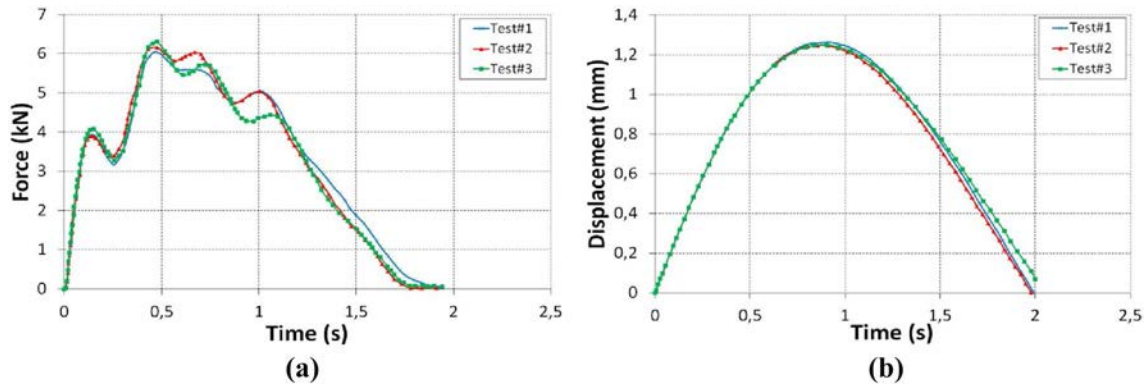


Fig. 12 The reproducibility of the force and displacement 5 J

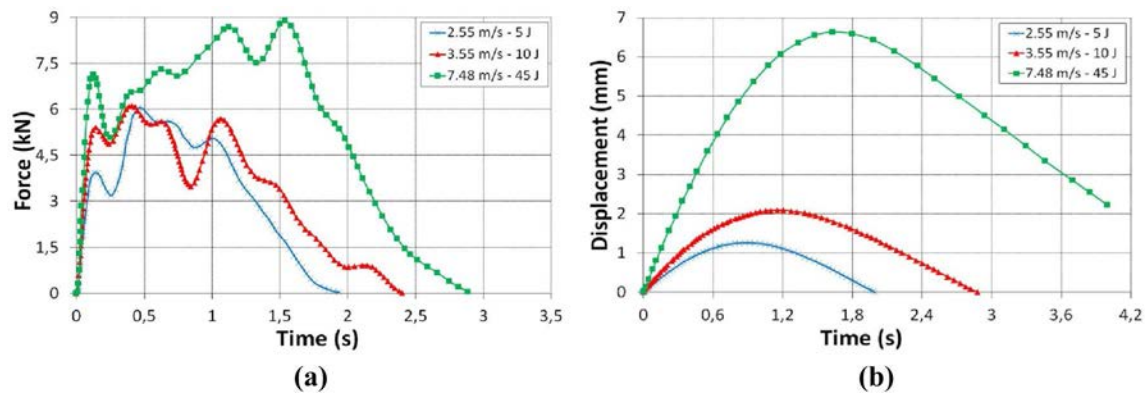


Fig. 13 Evolution of contact Force and displacement with impact energy

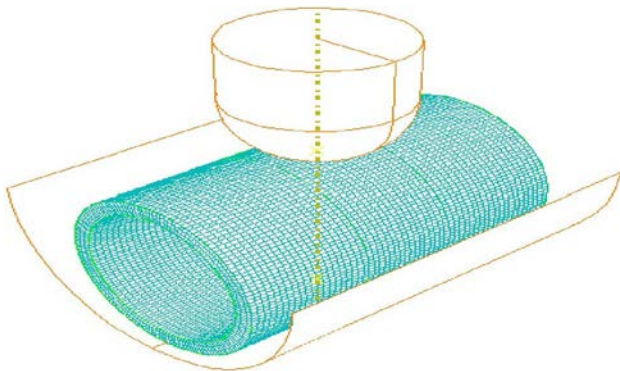


Fig. 14 Impact model for numerical simulation

Figure 19 shows a decrease in the velocity of the projectile with the time during the impact. The general appearance of these curves describes two phases of speed variation during impact. In the first phase, the impactor is severely hampered by the wind turbine blade and loses much of its kinetic energy which is converted into deformation energy, which explains the rapid decrease observed in the speed of

Table 7 Tube characteristics

Diameter (mm)	55
Thickness (mm)	6
Length (mm)	200
Winding	$[\pm 55]_{10}$
Structure type	Solid
Mesh type	C3D8R
Mesh size (mm)	6
Number of elements	2079

the impactor to zero velocity corresponding to the start of the phase of elastic return. The second phase begins with the rebound of the impactor due to the elastic properties of the structure.

Figure 20 shows the force–time curves versus impact velocity for different impact scenarios. The effects of impactor shape, weight, and velocity are noticeable. The maximum force corresponding to the Hemispherical projectile is 100 kN at the tip of the blade and 89 kN at the trailing edge.

Two phases of force variation were noticed; initially, the evolution was linear till it reaches the peak force

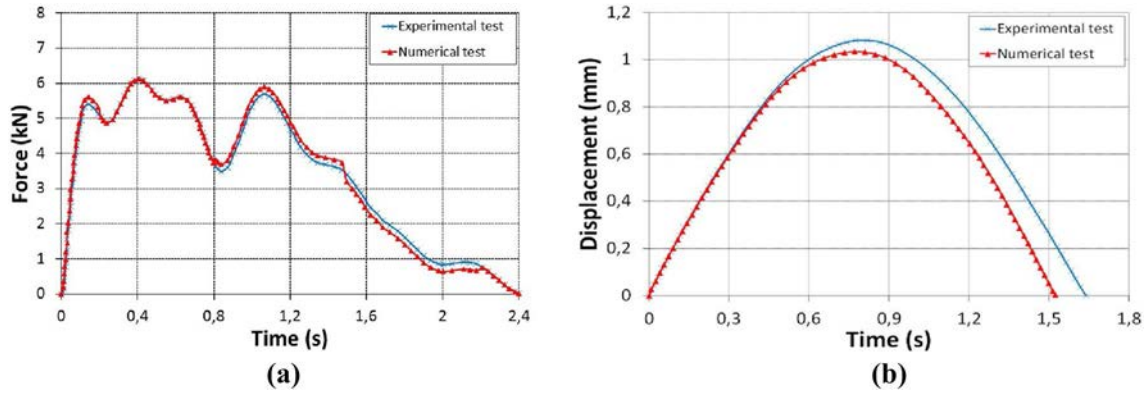


Fig. 15 Comparison of experimental and numerical results, $V = 2.55 \text{ m/s} - 5 \text{ J}$

(corresponds to 0 m/s) and then became non-linear due to the damage initiation. In the literature, during impact without damage, the force–time history has a parabolic symmetrical curve. Hence, the loading and unloading phases are identical. During impact with the wind turbine blade, the force–time curves show no symmetry between loading and unloading phases, due to damage initiation which is noted by the intense decline of the force with some oscillations. Then, the start of the damage evolution of composites until the complete failure of the structure.

The results show damages in some layers at both zones for the two impactors. Hashin criterion for matrix in tension (HSNMTCRT) has been reached. On the other hand, Hashin criterion for matrix in compression (HSNMCCRT), for fiber in tension (HSNFTCRT), and for fiber in compression (HSNFCCRT) condition is not yet verified as shown in Figs. 21, 22, 23, and 24.

The damage on the wind turbine blade occurred only after reaching the specific energy threshold which depends on

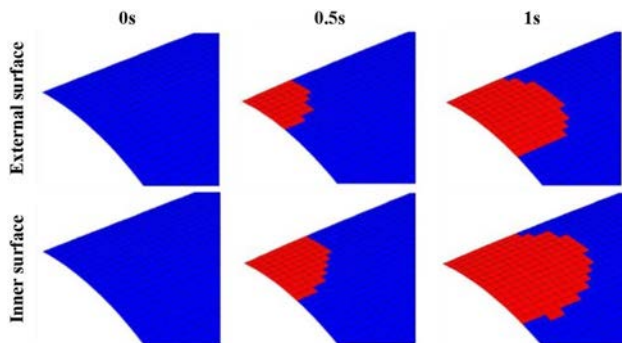


Fig. 16 The appearance of the damaged zone on the tube, $V = 2.55 \text{ m/s} - 5 \text{ J}$

the mechanical properties of the composite material used as well as on the boundary conditions applied to the structure.

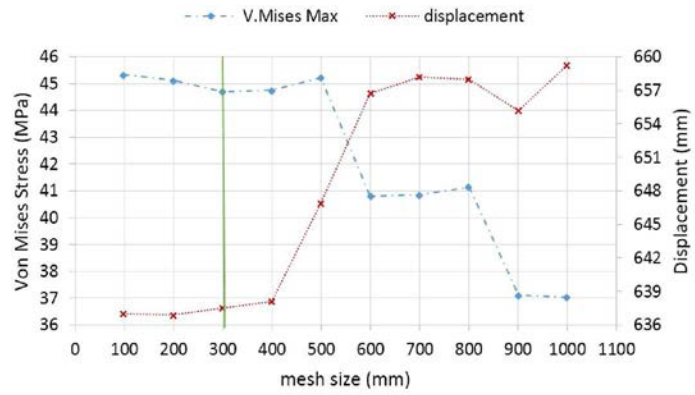
A close-up view of the impacted areas shows that the size of the damaged zone depends on the impactor geometry, weight, as well as on impact location. Impact with hemispherical projectile generates large damaged zone, while a very localized damage with penetration was observed with a conical impactor, e.g., as shown in Table 9, for an impact with 1 kJ at the tip of the blade, the damaged area is 0.34 m^2 for conical impactor; however, for the hemispherical projectile, it is about 0.497 m^2 . The same goes for heavier impactors; however, fast impactor generates violent impact force.

For identical impactor parameters, the impact force and the size of the damaged area registered at the tip of the blade are higher than the ones recorded at the trailing edge, which is due to the lamination model and the thickness of the materials. Furthermore, it was noted that the blade reaction to the impact at low speed is governed by flexion and a fraction of the incident energy was absorbed by the wind turbine blade and restored elastically to the impactor which led to its rebound, correlating with the results of impact study on current marine turbine nozzle [21].

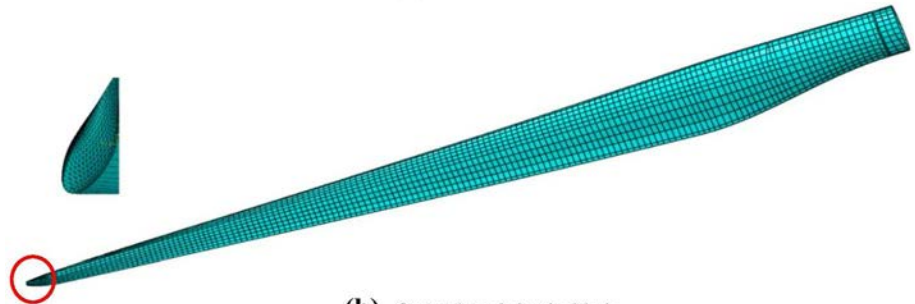
4 Conclusion

In this investigation, the numerical simulation of damage progressive in composite offshore wind turbine blade was tested. A VUMAT subroutine was developed and validated using both experimental and numerical simulations on a tubular specimen. The results show that numerical simulation could be considered as a powerful tool to reproduce the experimental approach and offers possibilities of predicting

Fig. 17 Study of the blade mesh convergence



(a) Mesh size study



(b) Optimal mesh for the blade

Table 8 Blade mesh study

Structure type	Shell deformable
Blade length m	48
Mesh element type	S4R
Mesh size mm	300
Number of elements	
Blade	5136
Blade with a conical impactor	5216
Blade with a Hemispheric impactor	5236

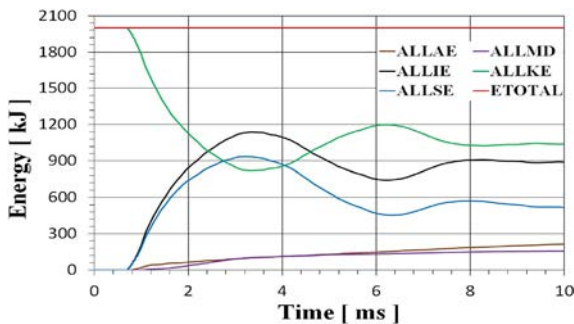


Fig. 18 Evolution of impact energies [5 kg–20 m/s]

failure modes and the mechanical response of a wind turbine blade under accidental impact by using the Finite Element Method.

The objective was to evaluate the effect of different parameters of impactor such as geometry, velocity, weight, and impact location on the mechanical behavior, type of damage, and its size on a composite wind turbine blade. Different impactor shapes have been considered for two impact velocities, and the effect of these parameters is noticeable. The variation of impact energy was controlled and analyzed and total energy conservation was satisfied.

The damage was controlled using Hashin’s criteria, and the main conclusions are given as follows: the damage evolution on the wind turbine blades depends on the stratification model. The maximum damaged area is obtained with a hemispherical impactor, while for the conical impactor the damage was more localized with indentation. Moreover, heaviest impactors had very slow elastic rebound. Finally, when rising the impactor velocity, the mechanical response of the wind turbine blade was governed by dilatation waves contrary to when impacted at low speed which was obviously dominated with an elastic rebound. The study of the damage phenomenon of wind turbine blades under impact has all its interest for the designer. Indeed, even a small scratch can have a considerable effect on the durability of the structure and will contribute to the rapid degradation of the structure.

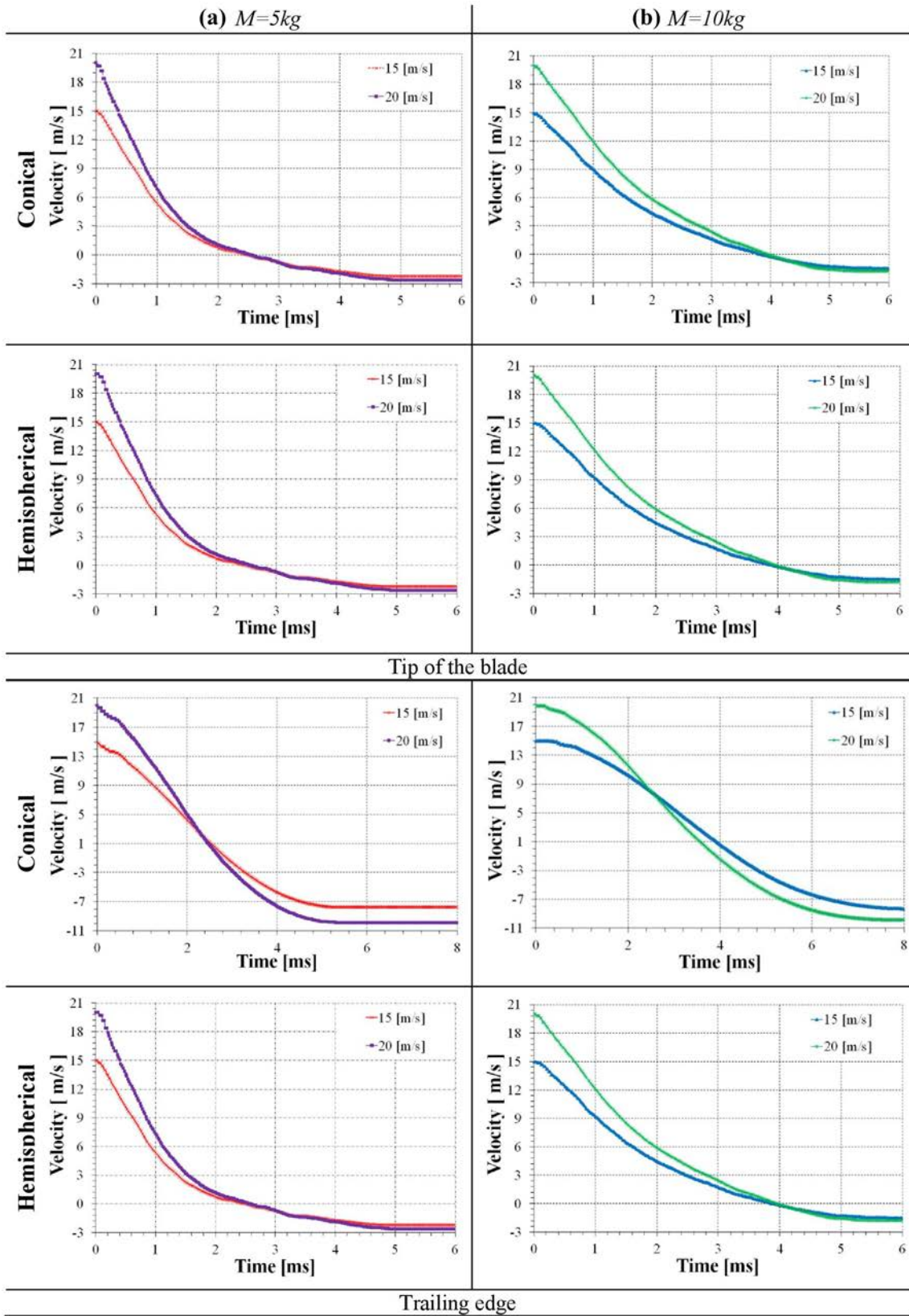


Fig. 19 Velocity–time curves vs. impact cases

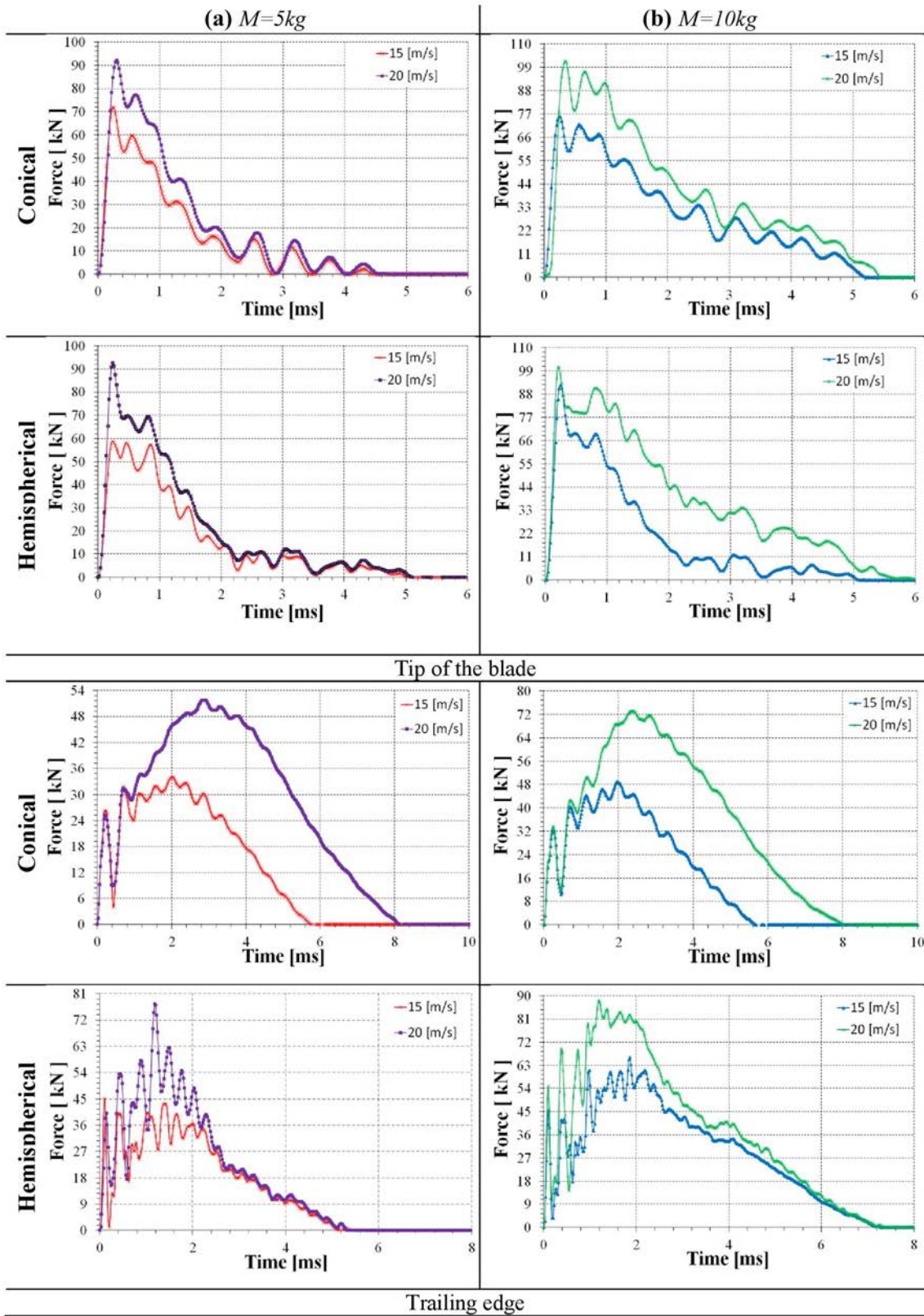


Fig. 20 Force–time curves vs. impact cases

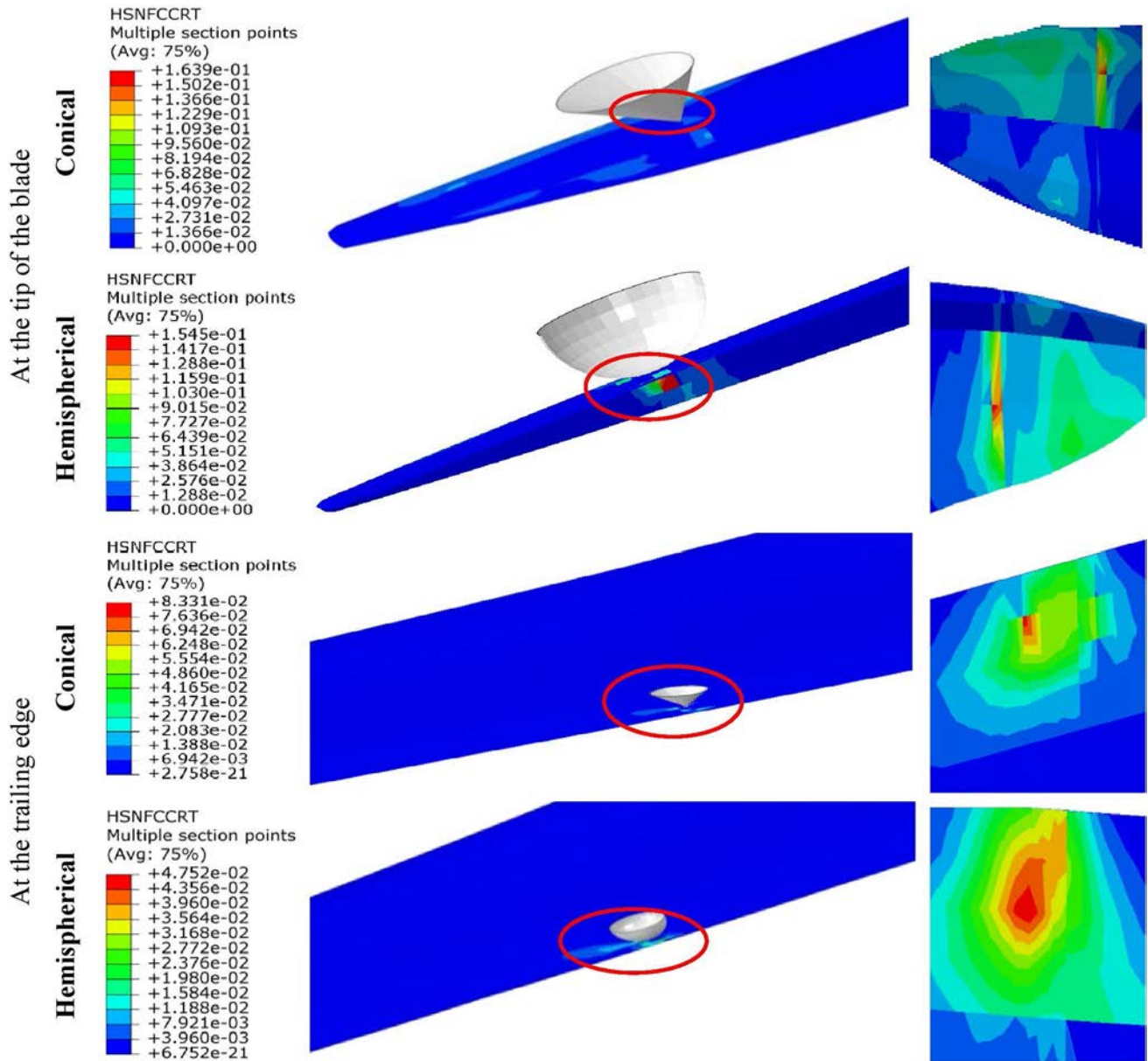


Fig. 21 Hashin fiber compressive criterion damages for impact at [M=10 kg, V=20 m/s]

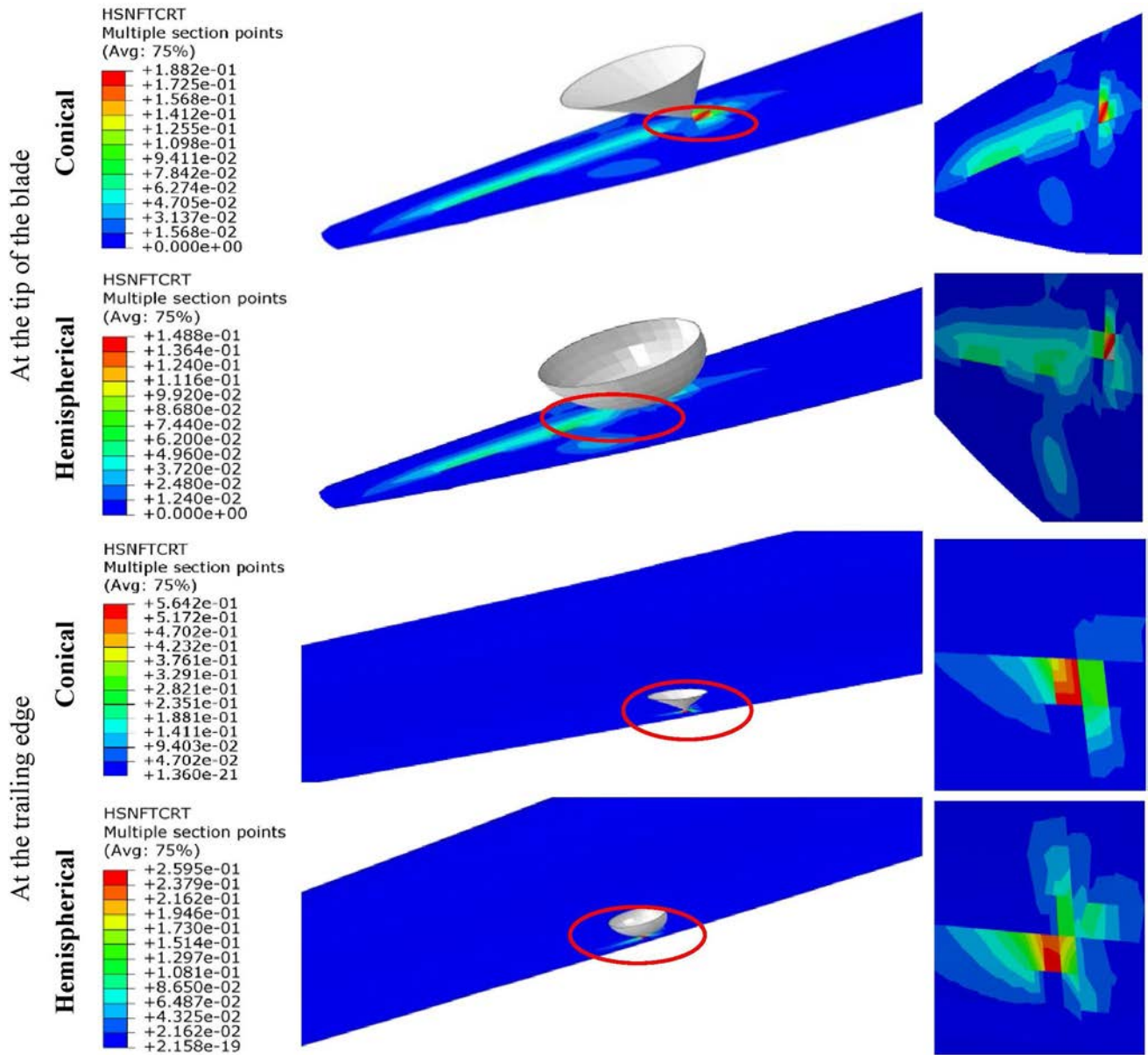


Fig. 22 Hashin fiber tensile criterion damages for impact at [M= 10 kg, V = 20 m/s]

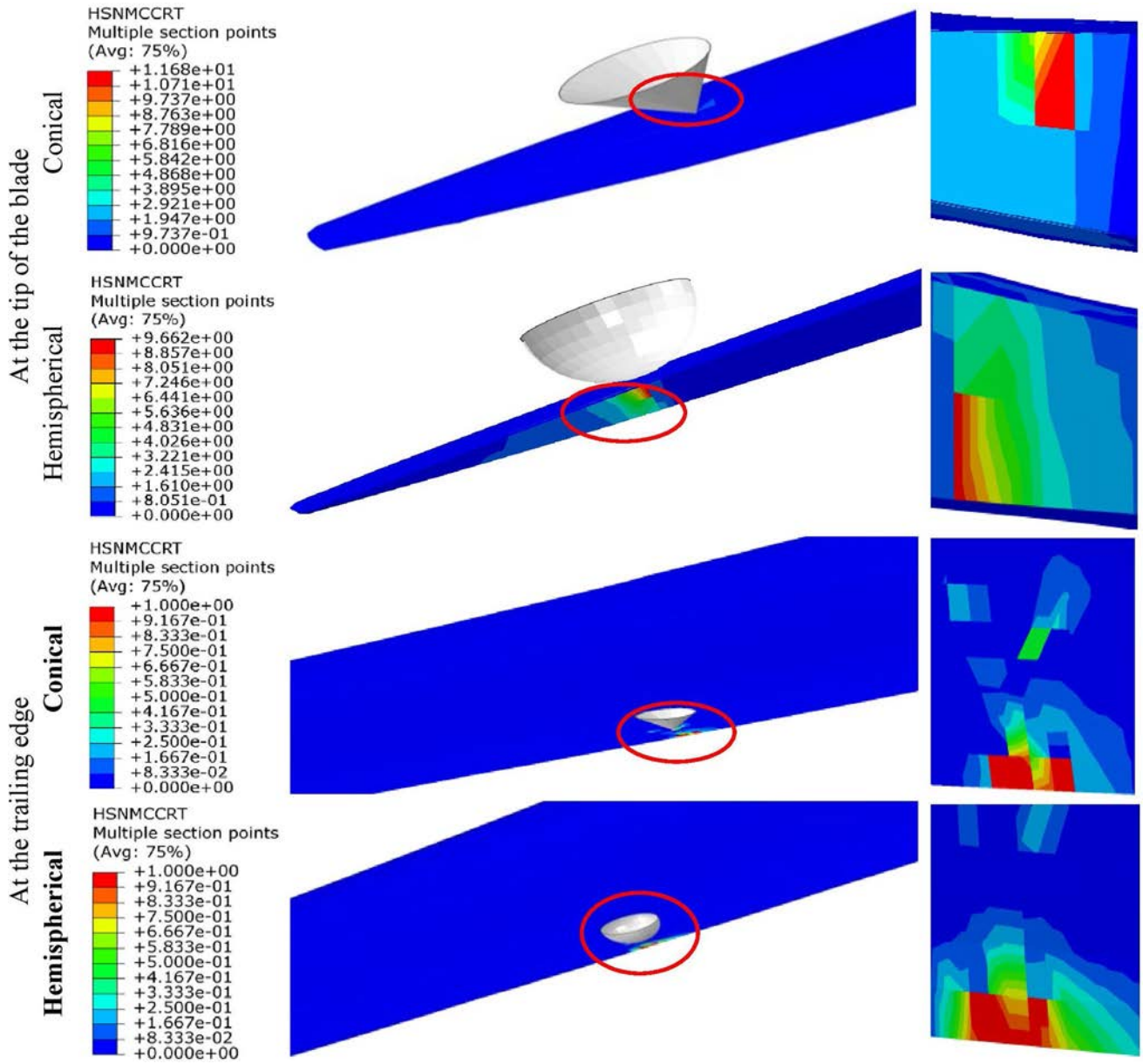


Fig. 23 Hashin matrix compressive criterion damages for impact at [M=10 kg, V=20 m/s]

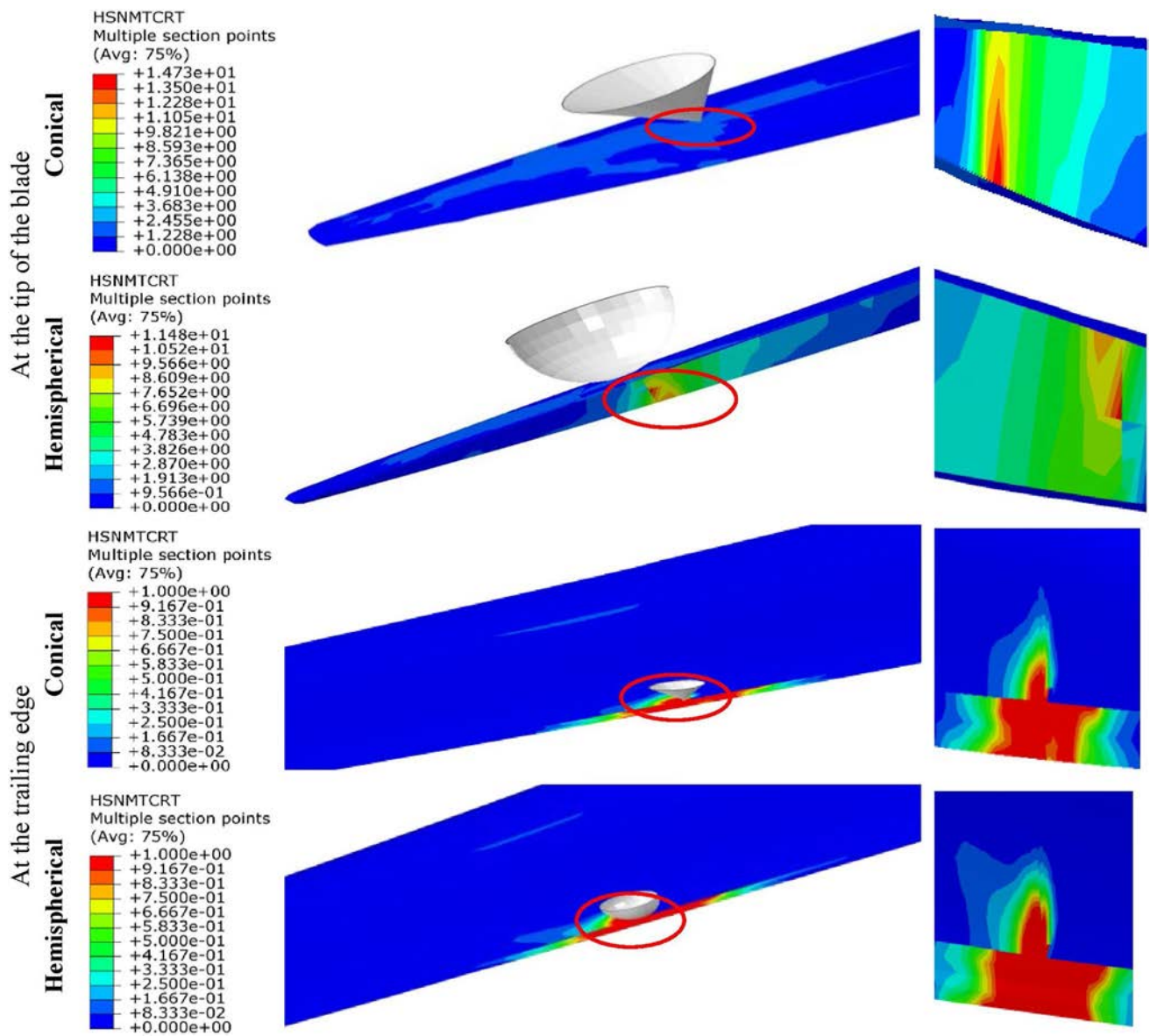


Fig. 24 Hashin matrix tensile criterion damage for impact at [M= 10 kg, V=20 m/s]

Table 9 Size of the damaged area(m²) with impact location and kinetic energy

	Conical				
	HSNFCCRT	HSNFCTCRT	HSNMCCRT	HSNMTCRT	Shear
47 m					
Energy [kJ]					
0.562	0	0	0	0.135	0.135
1.00	0	0	0.0075	0.3425	0.3425
1125	0	0	0.0075	0.3825	0.3825
2.00	0	0	0.0225	0.485	0.485
16 m					
Energy [kJ]					
0.562	0	0	0	0.0425	0.0425
1.00	0	0	0	0.06	0.06
1125	0	0	0	0.08	0.08
2.00	0	0	0.005	0.21	0.21
	Hemispherical				
	HSNFCCRT	HSNFCTCRT	HSNMCCRT	HSNMTCRT	Shear
47 m					
Energy [kJ]					
0.562	0	0	0	0.27	0.27
1.00	0	0	0.0075	0.4975	0.4975
1125	0	0	0.0075	0.575	0.575
2.00	0	0	0.0225	0.83	0.83
16 m					
Energy [kJ]					
0.562	0	0	0	0.075	0.075
1.00	0	0	0	0.1325	0.1325
1125	0	0	0	0.17	0.17
2.00	0	0	0.015	0.38	0.38

Compliance with Ethical Standards

Conflict of interest On behalf of all authors, the corresponding author states that there is no conflict of interest.

References

- Boudounit H, Tarfaoui M, Saifaoui D, Nachtane M (2020) Structural analysis of offshore wind turbine blades using finite element method. *Wind Eng* 44(2):168–180
- Renewable energy benefits leveraging local capacity for offshore wind, <https://www.irena.org/publications/2017/May/Leveraging-Local-Capacity-for-OffshoreWind> (Consulted le 19 September 2018).
- Renewable energy benefits leveraging local capacity for offshore wind, <https://www.irena.org/publications/2018/May/Leveraging-Local-Capacity-for-OffshoreWind> (Consulted le 19 September 2018).
- Schubel PJ, Crossley RJ, Boateng EKG, Hutchinson JR (2013) Review of structural health and cure monitoring techniques for large wind turbine blades. *Renew Energy* 51:113–123
- Schubel PJ, Crossley RJ (2012) Wind turbine blade design. *Energies* 5(9):3425–3449
- Dehouck V, Lateb M, Sacheau J, Fellouah H (2018) Application of the blade element momentum theory to design horizontal axis wind turbine blades. *J Sol Energy Eng* 140(1):014501
- Mulugeta BA, Gerawork A (2017) Aerodynamic design of horizontal axis wind turbine blades. *FME Trans* 45(4):647–660
- Shen X, Zhu X, Du Z (2011) Wind turbine aerodynamics and loads control in wind shear flow. *Energy* 36(3):1424–1434
- Bottasso CL, Campagnolo F, Petrović V (2014) Wind tunnel testing of scaled wind turbine models: beyond aerodynamics. *J Wind Eng Ind Aerodyn* 127:11–28
- Brøndsted P, Lilholt H, Lystrup A (2005) Composite materials for wind power turbine blades. *Annu Rev Mater Res* 35:505–538
- Sørensen BF, Jørgensen E, Debel CP, Jensen FM, Jensen HM, Jacobsen TK, Halling KM (2004) Improved design of large wind turbine blade of fibre composites based on studies of scale effects (Phase 1) Summary Report (Risø-R Report). Risø National Laboratory.
- Shokrieh MM, Rafiee R (2006) Simulation of fatigue failure in a full composite wind turbine blade. *Compos Struct* 74(3):332–342
- Montesano J, Chu H, Singh CV (2016) Development of a physics-based multi-scale progressive damage model for assessing the durability of wind turbine blades. *Compos Struct* 141:50–62

14. Montesano J, McCleave B, Singh CV (2018) Prediction of ply crack evolution and stiffness degradation in multidirectional symmetric laminates under multiaxial stress states. *Compos B* 133:53–67
15. Yang J, Peng C, Xiao J, Zeng J, Xing S, Jin J, Deng H (2013) Structural investigation of composite wind turbine blade considering structural collapse in full-scale static tests. *Compos Struct* 97:15–29
16. Overgaard LC, Lund E, Thomsen OT (2010) Structural collapse of a wind turbine blade. Part A: static test and equivalent single layered models. *Compos Part A* 41(2):257–270
17. Overgaard LCT, Lund E (2010) Structural collapse of a wind turbine blade. Part B: progressive interlaminar failure models. *Compos Part A* 41(2):271–283
18. Kennedy CR, Leen SB, ÓBrádaigh CM (2016) Immersed fatigue performance of glass fibre-reinforced composites for tidal turbine blade applications. *J Bio Tribo Corros* 2:12. <https://doi.org/10.1007/s40735-016-0038-z>
19. Tarfaoui M, Nachtane M, Khadimallah H, Saifaoui D (2017) Simulation of mechanical behavior and damage of a large composite wind turbine blade under critical loads. *Appl Compos Mater* 25:1–18
20. Lin CC, Lee YJ (2004) Stacking sequence optimization of laminated composite structures using genetic algorithm with local improvement. *Compos Struct* 63(3–4):339–345
21. Boudounit H, Tarfaoui M, Saifaoui D (2020) Modal analysis for optimal design of offshore wind turbine blades. *Mater Today: Proceedings* 30:998–1004. <https://doi.org/10.1016/j.matpr.2020.04.373>
22. Tarfaoui M, Nachtane M, Boudounit H (2020) Finite element analysis of composite offshore wind turbine blades under operating conditions. *J Therm Sci Eng Appl* 12(1):4042123
23. Tarfaoui M, Nachtane M, Shah OR, Boudounit H (2019) Numerical study of the structural static and fatigue strength of wind turbine blades. *Mater Today* 13:1215–1223
24. Boudounit H, Tarfaoui M, Saifaoui D (2019) Structural design and analysis of a 5mw offshore wind turbine blades under critical aerodynamic loads. 14th Congress of Mechanics, April 16–19, 2019 (Rabat, MOROCCO)
25. Boudounit H, Tarfaoui M, Saifaoui D (2017) Étude numérique d'une pale composite d'une éolienne flottante en service. 13ème Congrès de mécanique - CMM, Apr 2017, Meknès, Maroc. [ffhal-01730071](https://doi.org/10.1007/978-3-319-61730-7_1)
26. Boudounit H, Saifaoui D (2020) Wind farm design approach: feasibility and optimization study-case of the Dakhla site in Morocco. *J Appl Sci Environ Stud* 3(1):26–36
27. Nachtane M, Tarfaoui M, El Moumen A, Saifaoui D (2017) Damage prediction of horizontal axis marine current turbines under hydrodynamic, hydrostatic and impacts loads. *Compos Struct* 170:146–157
28. Nachtane M, Tarfaoui M, Saifaoui D, El Moumen A, & Boudounit H (2017) Caractérisation mécanique d'une hydrolienne en matériau composite dans un environnement marin.
29. Geubelle PH, Baylor JS (1998) Impact-induced delamination of composites: a 2D simulation. *Compos B* 29(5):589–602
30. E. Troussel (2013) Prédiction des dommages d'impact basse vitesse et basse énergie dans les composites à matrice organique stratifiés. Thèse de doctorat, Ecole nationale supérieure d'arts et métiers-ENSAM.
31. Hamitouche L, Tarfaoui M, Vautrin A (2008) An interface debonding law subject to viscous regularization for avoiding instability: application to the delamination problems. *Eng Fract Mech* 75(10):3084–3100
32. Pugh K, Rasool G, Stack MM (2018) Some thoughts on mapping tribological issues of wind turbine blades due to effects of onshore and offshore raindrop erosion. *J Bio Tribo Corros* 4:50. <https://doi.org/10.1007/s40735-018-0165-9>
33. Pugh K, Rasool G, Stack MM (2019) Raindrop erosion of composite materials: some views on the effect of bending stress on erosion mechanisms. *J Bio Tribo Corros* 5:45. <https://doi.org/10.1007/s40735-019-0234-8>
34. Ahamed RAR, Johnstone CM, Stack MM (2016) Impact angle effects on erosion maps of GFRP: applications to tidal turbines. *J Bio Tribo Corros* 2:14. <https://doi.org/10.1007/s40735-016-0044-1>
35. Abrate S (2001) Modeling of impacts on composite structures. *Compos Struct* 51(2):129–138
36. Davies GAO, Zhang X (1995) Impact damage prediction in carbon composite structures. *Int J Impact Eng* 16:149–170
37. Davies GAO, Olsson R (2004) Impact on composite structures. *Aeronaut J* 108:541–563
38. Olsson R (2000) Mass criterion for wave controlled impact response of composite plates. *Compos A* 31(8):879–887
39. Mitrevski T, Marshall I, Thomson R (2006) The influence of impactor shape on the damage to composite laminates. *Compos Struct* 76(1):116–122
40. Yamada SE, Sun CT (1978) Analysis of laminate strength and its distribution. *J Compos Mater* 12:275–284
41. L. J. Hart-Smith (1989) A new approach to fibrous composite laminate strength prediction. eighth DOD/NASA/FAA conference on fibrous composites in structural design, NASA CP-3087, Part 2, pp. 663–693. 3.
42. Hashin Z (1980) Failure criteria for unidirectional fiber composites. *J Appl Mech* 47(329–334):4